Cancer Research

Preclinical Efficacy of the Auristatin-Based Antibody–Drug Conjugate BAY 1187982 for the Treatment of FGFR2-Positive Solid Tumors

Anette Sommer[1], Charlotte Kopitz[1], Christoph A. Schatz[1], Carl F. Nising[2], Christoph Mahlert[2], Hans-Georg Lerchen[2], Beatrix Stelte-Ludwig[2], Stefanie Hammer[1], Simone Greven[2], Joachim Schuhmacher[2], Manuela Braun[1], Ruprecht Zierz[1], Sabine Wittemer-Rump[1], Axel Harrenga[3], Frank Dittmer[2], Frank Reetz[1], Heiner Apeler[2], Rolf Jautelat[2], Hung Huynh[4], Karl Ziegelbauer[1], and Bertolt Kreft[1]

Abstract

The fibroblast growth factor receptor FGFR2 is overexpressed in a variety of solid tumors, including breast, gastric, and ovarian tumors, where it offers a potential therapeutic target. In this study, we present evidence of the preclinical efficacy of BAY 1187982, a novel antibody–drug conjugate (ADC). It consists of a fully human FGFR2 monoclonal antibody (mAb BAY 1179470), which binds to the FGFR2 isoforms FGFR2-IIIb and FGFR2-IIIc, conjugated through a noncleavable linker to a novel derivative of the microtubule-disrupting cytotoxic drug auristatin (FGFR2-ADC). In FGFR2-expressing cancer cell lines, this FGFR2-ADC exhibited potency in the low nanomolar to subnanomolar range and was more than 100-fold selective against FGFR2-negative cell lines. High expression levels of FGFR2 in cells correlated with efficient internalization, efficacy, and cytotoxic effects *in vitro*. Pharmacokinetic analyses in mice bearing FGFR2-positive NCI-H716 tumors indicated that the toxophore metabolite of FGFR2-ADC was enriched more than 30-fold in tumors compared with healthy tissues. Efficacy studies demonstrated that FGFR2-ADC treatment leads to a significant tumor growth inhibition or tumor regression of cell line–based or patient-derived xenograft models of human gastric or breast cancer. Furthermore, *FGFR2* amplification or mRNA overexpression predicted high efficacy in both of these types of *in vivo* model systems. Taken together, our results strongly support the clinical evaluation of BAY 1187982 in cancer patients and a phase I study (NCT02368951) has been initiated. *Cancer Res; 76(21); 6331–9. ©2016 AACR.*

Introduction

Antibody–drug conjugates (ADC) represent a promising therapeutic approach for cancer treatment (1, 2). These agents combine the specificity of a monoclonal antibody directed against a cell surface antigen with the targeted delivery of a highly potent cytotoxic drug. Stable conjugation and specific targeting result in the accumulation of high local concentrations of cytotoxic agents that would not be tolerable if administered systemically. Currently, there are more than 40 ADCs in phase I/II of clinical development. Most of these contain a microtubule-destabilizing payload, either of the auristatin or the maytansine class (3). In addition, other payload classes, including DNA targeting pyrrolobenzodiazepines, indolinobenzodiazepine pseudodimers, duocarmycins, calicheamicins, as well as others derived from traditional chemotherapeutics, such as camptothecin and doxorubicin (4, 5), are currently under preclinical and clinical evaluation.

FGFR2 (fibroblast growth factor receptor 2) is a receptor tyrosine kinase with an important role in both embryonic development and tissue repair (6). Alternative gene splicing of the C-terminal half of the Ig-like domain III yields FGFR2 isoforms IIIb and IIIc exhibiting different ligand-binding specificities as well as distinctive expression profiles (6). *FGFR2* aberrations have been implicated in multiple cancer types, associated with poor prognosis and resistance to cancer treatments. Oncogenic FGFR2 functions, promoted by FGFR2 overexpression, gene amplification, gene fusions, and autoactivating mutations of the receptor, have been described in several cancers, including gastric, breast, and ovarian cancer (7–14). *FGFR2* gene amplification is found in 4% of triple-negative breast cancers (TNBC) and appears to promote breast tumorigenicity by maintaining breast tumor–initiating cells (11, 14). In gastric cancer, *FGFR2* is amplified in 5% to 10% of tumors, and FGFR2 mRNA overexpression is associated with poor overall survival (9). Both the prominent expression of FGFR2 in several cancers and the low cell surface expression in normal tissues render FGFR2 a particularly promising target for an ADC.

Herein, we introduce a novel ADC, BAY 1187982, consisting of a fully human FGFR2-specific monoclonal antibody BAY 1179470 conjugated via lysine side chains and a noncleavable linker to an innovative, highly potent microtubule-disrupting

[1]Bayer Pharma AG, Berlin, Germany. [2]Bayer Pharma AG, Wuppertal, Germany. [3]Bayer Intellectual Property GmbH, Monheim, Germany. [4]National Cancer Center Singapore, Division of Cellular & Molecular Research, Singapore.

Note: Supplementary data for this article are available at Cancer Research Online (http://cancerres.aacrjournals.org/).

A. Sommer and C. Kopitz contributed equally to this study.

Corresponding Author: Anette Sommer, Bayer Pharma AG, Müllerstr. 178, Berlin13353, Germany. Phone: 49-30-468-17974; Fax: 49-30-468-97974; E-mail: anette.sommer@bayer.com

doi: 10.1158/0008-5472.CAN-16-0180

auristatin W derivative (15, 16). We show that FGFR2-ADC BAY 1187982 is highly potent and selective *in vitro*, is stable in circulation, and exhibits strong tumor enrichment *in vivo*. Furthermore, it demonstrates remarkable antitumor activity in breast, gastric, and ovarian cancer models including patient-derived xenograft (PDX) models.

Materials and Methods

Cells

SNU-16, KATO III, 4T1, MDA-MB-231, and NCI-H716 cells were obtained from ATCC; KYSE-180 and CACO-2 from DSMZ; MFM-223 from ECACC; SUM-52PE from Asterand; and MDR1-LLC1 from Prof. A. H. Schinkel from the Netherlands Cancer Institute (Amsterdam, The Netherlands). Cancer cell lines were obtained between 2002 and 2012 and they were authenticated using short tandem repeat (STR) DNA fingerprinting by the DSMZ before using them in the experiments. Cells were maintained in an incubator at 5% CO_2, 90% humidity, and 37°C in standard cell culture media as indicated by provider.

Preparation and characterization of FGFR2 antibody BAY 1179470

The discovery of the FGFR2-specific antibody (FGFR2-Ab BAY 1179470) using the n-CoDeR Fab phage library (BioInvent International AB; refs. 17, 18), the expression, purification, and characterization of the Fab precursor and the FGFR2-Ab are described in Supplementary Methods. The FGFR2-Ab (BAY 1179470) bound specifically to FGFR2-positive cells in fluorescence-activated cell-sorting (FACS) experiments, induced internalization into FGFR2-positive cells, and resulted in FGFR2 degradation as observed in an FGFR2 ELISA. Colocalization of the internalized FGFR2-Ab was analyzed with immunocytochemistry and also by a quantitative detection performed with amnis FlowSight imaging flow cytometer. Details of the internalization and localization experiments are described in Supplementary Methods and below.

Preparation, characterization, and *in vitro* cytotoxicity of the FGFR2-ADC BAY 1187982

Preparation of the FGFR2-ADC BAY 1187982 is explained in Supplementary Methods. The microtubule-depolymerizing activity of the main toxophore metabolite (BAY 1168650) of FGFR2-ADC BAY 1187982 and the induction of apoptosis were analyzed *in vitro* in microtubule polymerization and caspase-3/7 assays, respectively, as explained in Supplementary Methods. CellTiter-Glo (CTG) Luminescent Cell Viability Assay (Promega) was used to determine the half maximal inhibitory concentration of cell viability (IC_{50}) in a panel of cancer cell lines. Cells (7,000 of SNU-16, KATO III, SUM-52PE, NCI-H716, and MFM-223 cells; 4,000 of MDA-MB-231 cells; 3,000 of KYSE-180 cells; and 750 of 4T1 cells per well) were seeded in 96-well plates and incubated for 24 hours. FGFR2-ADC BAY 1187982 or a control ADC (BAY 1160535), consisting of the isotype control Ab BAY 1138806 and the same linker toxophore as the FGFR2-ADC BAY 1187982, were added and the plates were incubated for 72 hours. Cell proliferation was quantified using the CTG assay according to manufacturer's instructions. The raw data were analyzed with a dose–response curve Analysis Spreadsheet developed by Bayer Pharma AG and Bayer Business Services on the IDBS (ID Business Solutions Ltd.) E-WorkBook Suite platform.

Detection of *FGFR2* amplification, mRNA, and protein expression in cancer cell lines and tumor models

To determine the FGFR2 receptor density, the number of antibodies bound per cell (ABC) was measured by flow cytometry in a panel of cancer cell lines as explained in Supplementary Methods. FGFR2 mRNA expression was determined by RNAscope 2.0 following the kit instructions from Advanced Cell Diagnostics using FGFR2 and PPIB (peptidyl prolyl isomerase B) target probes (19). RNA expression was scored according to kit instructions. RNAscope *H* score 0–400 was calculated as predominant intensity score multiplied by percentage of tumor cells with RNA signal. To analyze *FGFR2* amplification, formalin-fixed, paraffin-embedded (FFPE) slides (3 μm) were pretreated and incubated with FISH probes FGFR2-20-RE and CHR10-10-GR from Empire Genomics. For analysis, red (*FGFR2*) and green (*CEN10*) dots were counted in 40 nuclei per slide. Samples with large clusters of *FGFR2* signal were scored as *FGFR2:CEN10* > 5.

Determination of toxophore metabolites in plasma, tumor, and organ samples

The concentration of the toxophore metabolite of FGFR2-ADC BAY 1168650 was analyzed by HPLC coupled to ionization/tandem mass spectrometer detection. Mouse plasma, tumor, or organ homogenates were spiked with 0.5 to 500 μg/L of BAY 1168650 and used for calibration.

Detection of *in vivo* efficacy of FGFR2-ADC BAY 1187982

All animal experiments were conducted in accordance with the German animal welfare law or Guide for the Care and Use of Laboratory Animals (NIH, Bethesda, MD) and approved by local authorities or with the Singapore animal welfare law and by SingHealth Animal Care Committee authorities. For the SNU-16 xenograft model, tumor cells (2×10^6) were injected subcutaneously to female NOD/SCID mice (Taconic M&B). For MFM-223 and NCI-H716 xenograft models, tumor cells (1×10^7 or 2×10^6, respectively) were injected subcutaneously to female NMRI *nu/nu* mice (Taconic M&B). Cell inoculation was supplemented with 50% Matrigel (Basement Membrane Matrix, BD Biosciences). For MFM-223 xenografts, mice were implanted with 17β-estradiol pellets (0.37 mg, 90-day release, Innovative Research of America) subcutaneously 1 day prior to the tumor cell inoculation.

For the PDX models BR1115, GA0114, GA0033, PA0787, and ES0199, tumor fragments were inoculated subcutaneously to female BALB/c nude mice (Beijing HFK Bioscience Co. Ltd.) at CrownBio. For BR1115 xenografts, mice received subcutaneous implantation of 17β-estradiol pellets (0.05 mg, 60-day release, Innovative Research of America) on the day of tumor inoculation. For OV30-0511A, GC10-0608, and GC12-0811 xenografts, tumors were inoculated subcutaneously to female (OV30-0511A) or male (GC10-0608 and GC12-0811) SCID mice (Animal Resources Centre) at the laboratory of Prof. Huynh Hung (NCC Singapore). MAXF 857 tumor fragments were inoculated subcutaneously to female NMRI *nu/nu* mice (Harlan Laboratories, BV, Venray 5804 AB) at Oncotest GmbH. MRL 2003100375 tumor cells (5×10^5) were suspended in 50% Cultrex ECM (Trevigen) and injected subcutaneously to female NOD/SCID mice (Harlan Laboratories) at Molecular Response Laboratories.

In all *in vivo* experiments, mice ($n = 5$–30 per group, see figure legends) were randomized according to primary tumor size

prior to treatment. Unless otherwise indicated, FGFR2-ADC BAY 1187982 and the control ADC were administered once weekly intravenously and unconjugated FGFR2-Ab twice weekly (intravenously). Doxorubicin (10 mg/kg; Sigma) was given every 2 weeks (intravenously). Vinorelbine (10 mg/kg; Actavis) and paclitaxel (24 mg/kg; Lapharm GmbH) were administered once weekly (intravenously). PBS was used as the vehicle control. Tumor volume [(length × width^2)/2] was measured by caliper at least twice weekly, and the treatment response was defined using the RECIST criteria (20). Progressive disease (PD) was defined as greater than 20% increase in tumor size. Partial response (PR) was defined as greater than 30% reduction in tumor size. Complete response (CR) was defined as an absence of any palpable tumor mass. No tumor growth or a slight reduction (<30%) or small increase (<20%) in tumor size was defined as stable disease (SD). Treatment-to-control ratios (T/C) were calculated on the basis of mean tumor volumes.

Ex vivo analyses on tumor samples

To determine total (t-FGFR2) and phosphorylated (P-FGFR2) FGFR2 in tumor lysates, tumors were cut into 5 × 5 mm^2 fragments, lysed and analyzed by Prometheus' collaborative enzyme enhanced reaction (CEER) assay (21). FGFR2 immunoblot analysis was performed on a panel of ovarian cancer PDX models. Tumor samples were lysed and separated on SDS-PAGE followed by blotting and incubation with the anti-FGFR2 rabbit

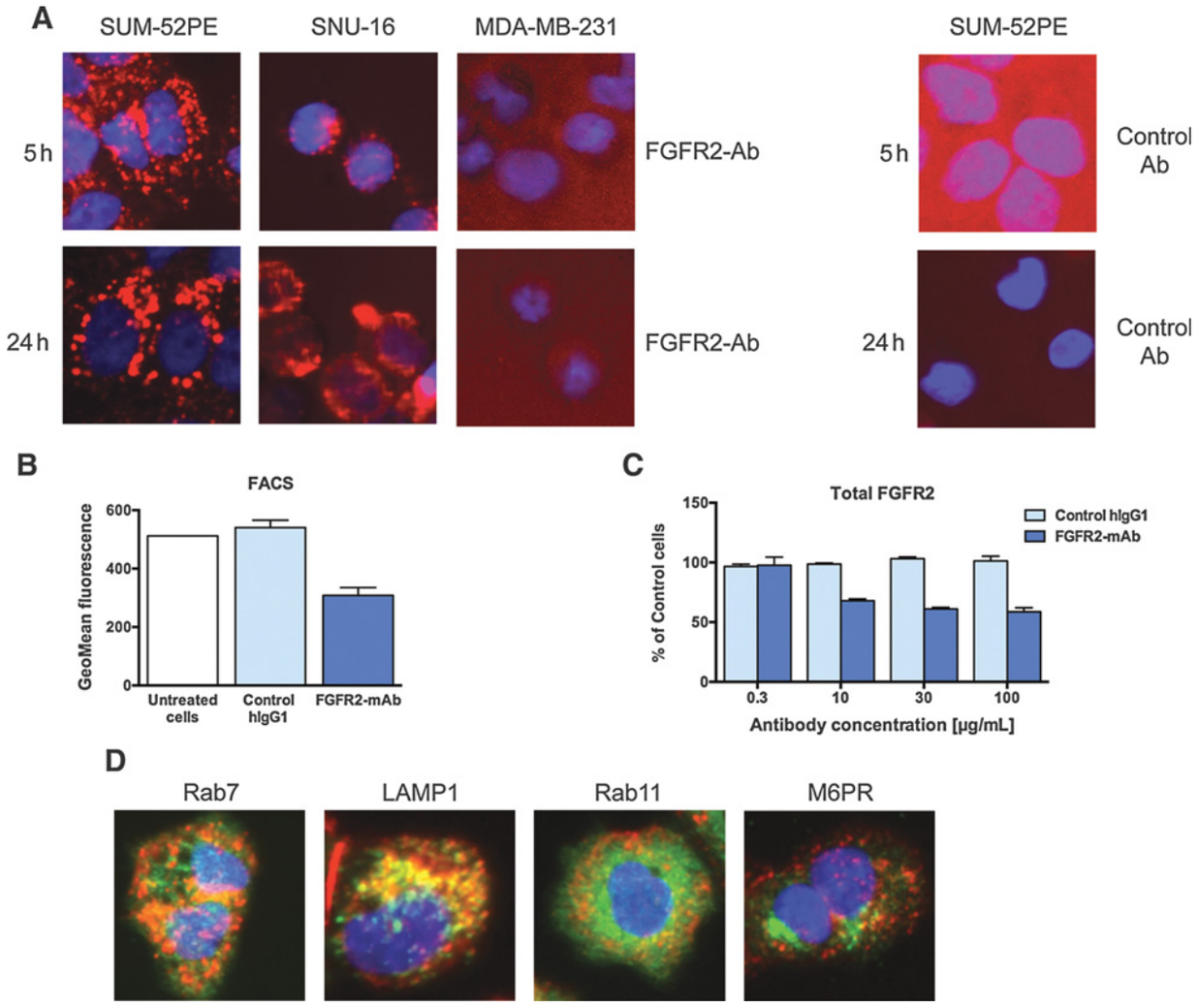

Figure 1.

The FGFR2-specific Ab (BAY 1179470) induces FGFR2 internalization and degradation *in vitro*. **A,** fluorescence immunocytochemistry was used to evaluate the FGFR2-Ab-induced internalization of FGFR2 in cells with high (SUM-52PE, SNU-16) or low (MDA-MB-231) FGFR2 expression (left) compared with isotype control Ab in SUM-52PE (right). **B,** FACS analysis of FGFR2 cell surface expression in SNU-16 gastric cancer cells upon incubation with 10 μg/mL of FGFR2-Ab for 5 hours at 37°C. White bar represents untreated control cells. One representative experiment of 3 independent experiments each performed in duplicates is shown. **C,** total FGFR2 levels upon incubation of SNU-16 cells with a predecessor antibody for BAY 1179470, FGFR2-Ab BAY 1138922, or isotype control Ab for 96 hours as determined by ELISA. One representative experiment of 2 independent experiments each performed in triplicates is shown. **D,** localization of Cypher5E-labeled FGFR2-Ab (red) 6 hours after incubation with live SUM-52PE cells and subsequent staining with anti-Rab7, -LAMP1, -Rab11, or -M6PR (green, respectively). Yellow regions indicate colocalization. Blue DNA stain in **A** and **D** indicates the nucleus.

polyclonal antibody Bek C-17 (sc-122) from Santa Cruz. To analyze the mode of action of BAY 1187982 *in vivo*, FFPE samples of the PDX model BR1115 were stained for phospho-histone H3 (pHH3, Ser10) as marker of mitotic cells with chromosomes in G_2–M phase, cleaved PARP1 as marker of apoptosis, and for α-tubulin to indicate tubulin structures as explained in Supplementary Methods.

Statistical analyses

For the comparison of t-FGFR2 and P-FGFR2, statistical significance was determined using Kruskal–Wallis test, followed by Mann–Whitney *U* test with Holm–Bonferroni correction. The comparison of final tumor weights was performed by one-way ANOVA, followed by a Dunnett test. For the final tumor volume, the log-transformed data were analyzed using one-way ANOVA and Tukey HSD test or Kruskal–Wallis test, followed by Mann–Whitney *U* test with Holm–Bonferroni correction. All analyses were compared to vehicle group and performed using statistical software R (version 3.1.2). $P < 0.05$ was considered statistically significant.

Results

Generation and characterization of the FGFR2-specific antibody

The monoclonal antibody BAY 1179470 (FGFR2-Ab) was selected because of its high binding affinity to the extreme N-terminus of human FGFR2 (K_d of 75 nmol/L) as detected by surface plasmon resonance, the critical residues being Pro-2, Leu-6, and Glu-8. The N-terminal epitope recognized by this FGFR2-Ab is present in all described FGFR2 splice variants and is 100% identical in human, rat, rhesus monkey, and murine FGFR2. Consequently, the selected FGFR2-Ab binds specifically to FGFR2 (but not FGFR1, FGFR3, or FGFR4) and shows a wide cross-species reactivity (EC_{50} of 0.25–0.35 nmol/L for mouse, rat, dog, pig, and rhesus monkey FGFR2 protein) allowing informative preclinical safety studies. Fluorescence microscopy analyses revealed that the FGFR2-Ab induced rapid internalization of FGFR2 in FGFR2-positive cancer cells (SUM-52PE, SNU-16), which was not observed in FGFR2-negative cancer cells (MDA-MB-231) or with an isotype control Ab (Fig. 1A). Antibody-mediated internalization was confirmed by FACS analysis and measurement of FGFR2 degradation by ELISA in SNU-16 cells (Fig. 1B and C, respectively). Internalized FGFR2-Ab colocalized with lysosomal Rab7 (early endosome marker) and LAMP1 (lysosomal-associated membrane protein 1) but not with recycling endosome marker Rab11 or late endosome marker M6PR (mannose-6-phosphate receptor), indicating that FGFR2-Ab induced FGFR2 intracellular trafficking will result in routing of FGFR2-Ab to the lysosome as shown also with immunocytochemistry (Fig. 1D) and lead to degradation of the antibody (Fig. 1C). The colocalization of FGFR2-Ab with the lysosomal marker LAMP1 or with the early endosome marker Rab7 was observed in approximately 60% of SUM-52PE cells as determined using imaging flow cytometer.

Generation of the FGFR2-targeting ADC BAY 1187982

To generate the FGFR2-ADC, FGFR2-Ab was coupled to a novel, highly potent *N*-methyl auristatin W derivative. Cysteine-linked ADCs with thiosuccinimide linkages can undergo deconjugation via retro-Michael reaction resulting in a partial loss of drug load *in vivo* (22). To achieve maximum stability and to avoid FGFR2-ADC deconjugation *in vivo*, the auristatin W was attached to lysine side chains of the Ab via an *N*-(5-carboxypentyl) linker (16). The *N*-(5-carboxypentyl)–modified auristatin W derivative was transformed into an activated *N*-hydroxy succinimide ester and was subsequently coupled to the FGFR2-Ab to generate the FGFR2-ADC BAY 1187982 (Fig. 2A) with an average drug-to-antibody ratio (DAR) of 4 (range, 1.7–5.1). Both the unconjugated antibody FGFR2-Ab and the FGFR2-ADC BAY 1187982 exhibited antigen-binding affinities of 0.29 nmol/L as determined by ELISA, indicating that linker payload conjugation does not affect the antigen recognition of the FGFR2-Ab *in vitro*.

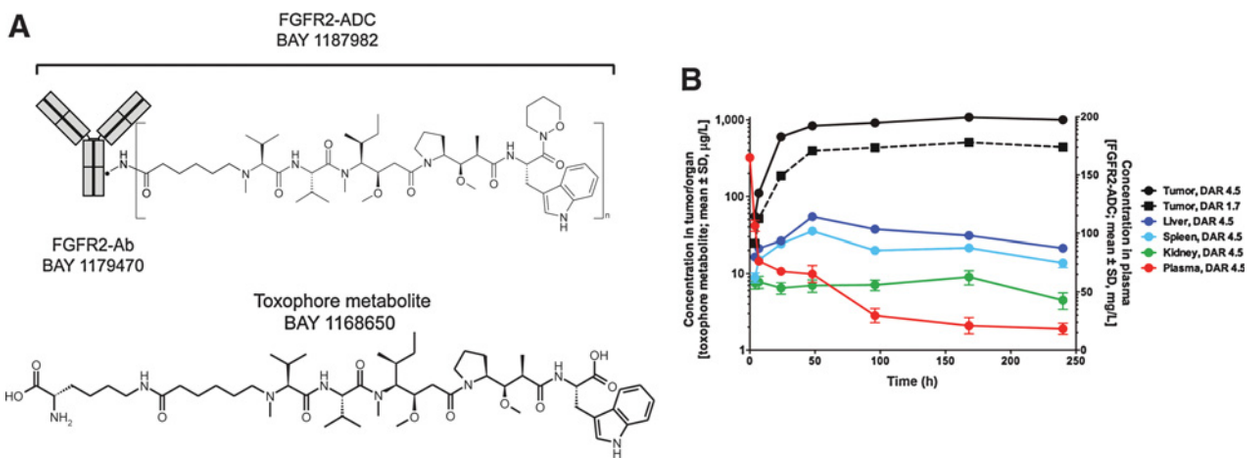

Figure 2.

Characteristics of FGFR2-ADC BAY 1187982. **A,** chemical structures of BAY 1187982 with a DAR of $n \sim 4$ and of the toxophore metabolite BAY 1168650. BAY 1179470 represents FGFR2-Ab. **B,** concentration of FGFR2-ADC in plasma and of toxophore metabolite BAY 1168650 in tumor, liver, spleen, and kidney after intravenous administration of 5 mg/kg BAY 1187982 with DAR 1.7 or DAR 4.5 in tumor-bearing (NCI-H716) female NMRI *nu/nu* mice. For FGFR2-ADC with DAR 1.7, only tumor concentration is presented.

In vitro cytotoxicity of BAY 1187982 is selective and correlates with FGFR2 expression levels

The microtubule-depolymerizing activity of the auristatin toxophore metabolite (BAY 1168650) of BAY 1187982 was first confirmed in an *in vitro* microtubule polymerization assay with toxophore linker metabolite (Supplementary Fig. S1A). *In vitro* cytotoxicity of BAY 1187982 was subsequently analyzed in a broad panel of cancer cell lines in comparison to the nonbinding control ADC containing an identical linker payload. To correlate *in vitro* potency with FGFR2 receptor density on the cell surface, the number of FGFR2 ABC count was determined for a panel of cancer cell lines by quantitative FACS analysis. High FGFR2 levels were observed in KATO III, SUM-52PE, NCI-H716, MFM-223, and SNU-16 cell lines (Supplementary Table S1). The ABC count, an indirect measure for cell surface FGFR2 expression, correlated well with the *in vitro* potency of FGFR2-ADC BAY 1187982 with IC_{50} values ranging from 0.097 to 0.83 nmol/L in cell lines harboring at least 10,000 antibody-binding sites. Importantly, BAY 1187982 was more than 100-fold selective compared with the nonbinding control ADC. Both caspase-3/7 activation assay and FACS-based cell-cycle analysis demonstrated that treatment with FGFR2-ADC, but not with the control ADC, activated caspase-3/7 and increased the number of cells with a sub-G_1 content in FGFR2-positive SNU-16, respectively. This was not observed in MDA-MB-231, which express very low levels of FGFR2 (Supplementary Fig. S1B and S1C), strongly indicating that FGFR2-ADC induces apoptosis *in vitro* specifically in FGFR2-positive cells.

BAY 1187982 treatment results in high intratumoral concentrations of its toxophore metabolite

Because the therapeutic effects of ADCs are dependent on the tumor-specific delivery of the toxophore, we next studied the concentration of the main toxophore metabolite BAY 1168650 in tumors, liver, kidneys, and spleen in NMRI *nu/nu* mice bearing NCI-H716 tumors following intravenous administration of 5 mg/kg FGFR2-ADC BAY 1187982 with a DAR of 1.7 or 4.5 (Fig. 2B). The plasma concentration values for BAY 1187982 with a DAR of 4.5 were C_{max} of 165 mg/L, AUC of 13,614 mg h/L, and $t_{1/2}$ of 196 hours. The respective values for BAY 1187982 with a DAR of 1.7 were in a comparable range ($C_{max} = 131$ mg/L, AUC = 13,345 mg *h/L, and $t_{1/2} = 182$ hours). The active toxophore metabolite BAY 1168650 was found to be enriched more than 30-fold in tumors versus normal tissues (liver, spleen, and kidneys) as expected because of the high FGFR2 expression level on NCI-H716 tumor cells. BAY 1187982 with DAR of 4.5 yielded an approximately 2-fold higher concentration of the toxophore metabolite in tumors as compared with the ADC with a DAR of 1.7. However, the tumor/organ ratio of the metabolite was independent of the DAR value of the BAY 1187982 with AUC ($0–t_{last}$) ratios 27.7 versus 26.6 in liver, 32.3 versus 41.0 in spleen, and 103.2 versus 125.3 for DAR 1.7 and 4.5, respectively. Importantly, there is no evidence that BAY 1187982 would exert a bystander effect, as the toxophore metabolite has a low membrane permeability in CACO-2 cells as well as in the P-glycoprotein–expressing MDR1-LLC1 cell line (data not shown).

BAY 1187982 treatment results in CRs in TNBC and PRs in gastric and colorectal cancer xenograft models

To analyze the *in vivo* efficacy of BAY 1187982, the FGFR2-ADC was first tested in the human SNU-16 gastric cancer xenograft model using two different DARs (1.8 and 4.5) and two treatment schedules (Q4D×3 and Q10D×3). In contrast to the control ADC, treatment with FGFR2-ADC BAY 1187982 at 5 mg/kg resulted in partial tumor regression in at least 90% of the animals irrespective of the DAR and treatment schedule used (Fig. 3A and B). Lower FGFR2-ADC doses of 0.5 or 1 mg/kg did not significantly inhibit tumor growth compared with the vehicle control. To further assess the duration of tumor growth inhibition induced by BAY 1187982 at 5 mg/kg, animals were maintained for additional 30 days without treatment. On day 62, tumor regrowth was evident in all BAY 1187982-treated animals (Fig. 3A). The antitumor activity of BAY 1187982 was selective, as the nontargeting control ADC had no apparent effect on tumor growth.

In a separate experiment using an intermediate dosing schedule of Q7D×3, the lowest dose sufficient to induce PR was determined as 1.25 mg/kg. Weekly administration of BAY 1187982 (Q7D×3) at 2.5, 5, and 10 mg/kg resulted in a significant inhibition of tumor growth including the induction of PRs ($P < 0.05$, Fig. 3C). Treatment with BAY 1187982 was well tolerated. The highest dose of 10 mg/kg resulted in 10.5% transient reduction of the mean body weight 4 days after start of therapy. Animals regained normal body weights within 1 week.

When tested in the MFM-223 TNBC model, BAY 1187982 treatment at 1 and 5 mg/kg resulted in a marked decrease in tumor volume ($P < 0.001$), similarly to the standard-of-care doxorubicin ($P = 0.001$, Fig. 3D and E). Moreover, BAY 1187982 at 5 mg/kg resulted in PRs in all mice, whereas the lower dose of 1 mg/kg was sufficient to achieve PRs in 6 of 10 mice (Fig. 3F). Similarly to our experiment with the SNU-16 cell line, neither the control ADC (Fig. 3D and E) nor the unconjugated FGFR2-Ab (antitumor activity with T/C ratio of 1.22) had an effect on tumor growth. Finally, the impact of different treatment schedules was also assessed in the MFM-223 model in which administration of BAY 1187982 at all doses resulted in strong antitumor effects as indicated by a high number of mice with CR ($P < 0.001$, Supplementary Fig. S2A and S2B).

Interestingly, the significant antitumor efficacy of BAY 1187982 correlated with a substantial decrease in t-FGFR2 and P-FGFR2 protein levels in MFM-223 tumors at the end of the experiment ($P < 0.001$, Fig. 3G). In contrast, the nontargeted control ADC showed variable effects on FGFR2 protein, with 5 mg/kg suppressing the t-FGFR2 level and 1 mg/kg leading to a minor increase in P-FGFR2 protein content in the tumor.

In addition to being highly effective in MFM-223 and SNU-16 models, FGFR2-ADC BAY 1187982 at 7.5 mg/kg resulted in notable inhibition of tumor growth also in another cell line–derived xenograft model overexpressing FGFR2, the NCI-H716 human colorectal cancer model ($P < 0.001$, Table 1). In this model, neither paclitaxel nor vinorelbine inhibited tumor growth (T/C ratios, 0.91 and 1.02, respectively).

BAY 1187982 is efficacious in several PDX models with *FGFR2* amplification and high mRNA expression

To further substantiate the antitumor efficacy of BAY 1187982, the FGFR2-ADC was evaluated in several PDX mouse models representing various cancer types with different FGFR2 expression and amplification level (Table 1).

In the ovarian cancer PDX model OV30-0511A, BAY 1187982 at 7.5 and 15 mg/kg led to a remarkable and specific inhibition of tumor growth with T/C values of 0.08 and 0.12, respectively ($P < 0.001$, Fig. 4A and B). Cisplatin and paclitaxel

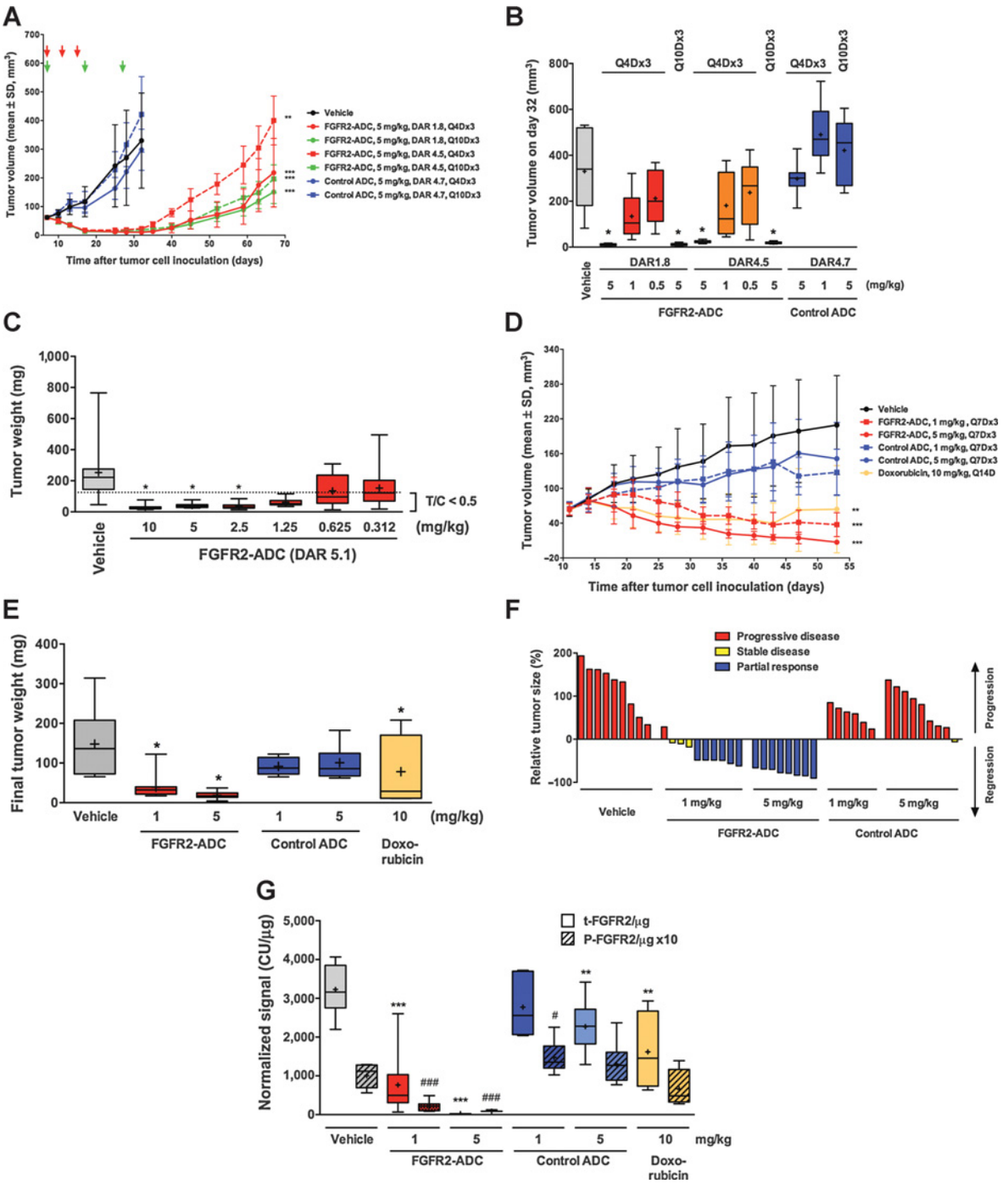

Figure 3.

Antitumor activity of FGFR2-ADC BAY 1187982 in SNU-16 human gastric cancer and MFM-223 human TNBC mouse models. **A** and **B,** for SNU-16 model ($n = 10$), treatment with FGFR2-ADC was started when tumor size had reached approximately 63 mm^3. **A,** tumor growth. Red and green arrows, treatment schedules with 4 (Q4D×3) and 10 days (Q10D×3) interval, respectively. **B,** tumor volume 32 days after tumor cell inoculation. **C,** for determining the MED in SNU-16 model ($n = 8$–10), treatment with FGFR2-ADC was started when tumors had reached a mean size of 48 mm^3. **D–G,** for MFM-223 model ($n = 4$–10), treatment with FGFR2-ADC (BAY 1187982 with DAR of 4.5) and doxorubicin was initiated when tumors had reached a size of 48 to 95 mm^3. **D,** tumor growth curves. **E,** final tumor weight. **F,** changes in tumor size represented as a percentage of the initial tumor size in each individual mouse. PD, mice exhibiting > 20% tumor growth; SD, mice exhibiting < 30% tumor shrinkage and <20% tumor growth; PR, mice exhibiting >30% tumor shrinkage. **G,** total (t-FGFR2) and phosphorylated (P-FGFR2) protein levels. The *y*-axis represents normalized CUs (normalized fluorescence units). Horizontal lines in box plots represent the 5th, 25th, 50th, 75th, and 95th centiles and crosses indicate mean values. Asterisks, statistical significance, analyzed by Kruskal–Wallis test, followed by Mann–Whitney *U* test (**A** and **D**), one-way ANOVA, followed by a Dunnett test (**B, C,** and **E**) or Kruskal–Wallis test, followed by Mann–Whitney *U* test with Holm–Bonferroni correction (**G**). *, $P < 0.05$; **, $P < 0.01$; ***, $P < 0.001$ when compared with the vehicle group. #, $P < 0.05$; ###, $P < 0.001$ when compared with vehicle for P-FGFR2. Q4D×3, every 4th day for three cycles; Q7D×3, every 7th day for three cycles; Q10×3, every 10th day for three cycles; Q14D, every 14 day.

Table 1. Antitumor efficacy of FGFR2-ADC BAY 1187982 (Q7D×3) in a panel of cell line- and patient-derived xenograft models shown as response rates and T/C values

Model	Cancer type	CDX/PDX	Dose, mg/kg	Response rate	T/C FGFR2-ADC	*FGFR2: CEN10*	FGFR2 RNAscope *H* score (0–400)
GA0033	Gastric	PDX	7.5	100% CR	0.00	>5	400
MFM-223[a]	TNBC	CDX	5[c]	91% CR, 9% PR	0.03	>5	400
OV30-0511A	Ovarian	PDX	7.5	43% SD, 57% PD	0.08	>5	400
SNU-16	Gastric	CDX	5[c]	100% PR	0.10	>5	400
NCI-H716	Colorectal	CDX	5	20% SD, 80% PD	0.24	>5	400
BR1115[b]	Breast	PDX	7.5	100% PD	0.37	>5	400
GA0114	Gastric	PDX	7.5	100% PD	0.56	>5	399
PA0787	Pancreatic	PDX	7.5	100% PD	0.43	1[d]	303
GC10-0608	Gastric	PDX	10	100% PD	0.27	0.6[d]	277
ES0199	Esophagus	PDX	7.5	100% PD	0.85	~1	252
KYSE-180	Esophagus	CDX	10	100% PD	0.95	n.d.	250
4T1 (murine)	Breast	CDX	7.5[c]	100% PD	0.79	n.d.	118[e]
MRL 2003100375	TNBC	PDX	12.5	60% PR, 20% SD, 20% PD	0.20	~1	61
GC12-0811	Gastric	PDX	10	100% PD	0.52	1	60
MAXF 857	TNBC	PDX	10	100% PR	0.01	~1[d]	45

NOTE: *FGFR2* amplification and mRNA expression of the models are listed.
Abbreviations: CDX, cell line–derived xenograft model; n.d., not determined; T/C, treatment versus control ratio; Q7D×3, every 7th day for three cycles.
[a]Response rate from the experiment shown as Supplementary Fig. S1B.
[b]*FGFR2-GAB2* fusion gene identified in BR1115 PDX model.
[c]BAY 1187982 administered every 4th day for 3 cycles (Q4D×3).
[d]Polysomal *FGFR2/CEN10*; MAXF857: 4.3/4.1; PA0787: 4.45/4.7; GC12-0811: 3.0/4.95.
[e]Scored at Bayer Pharma AG with human FGFR2-specific RNAscope probe, which is cross-reactive with murine FGFR2.

showed only moderate antitumor efficacy with T/C values of 0.35 and 0.38, respectively. OV30-0511A–bearing mice were sensitive to vinorelbine, which showed comparable efficacy as BAY 1187982 with a T/C value of 0.14. These tumors exhibited strong *FGFR2* amplification and high FGFR2 protein expression (Fig. 4C and D).

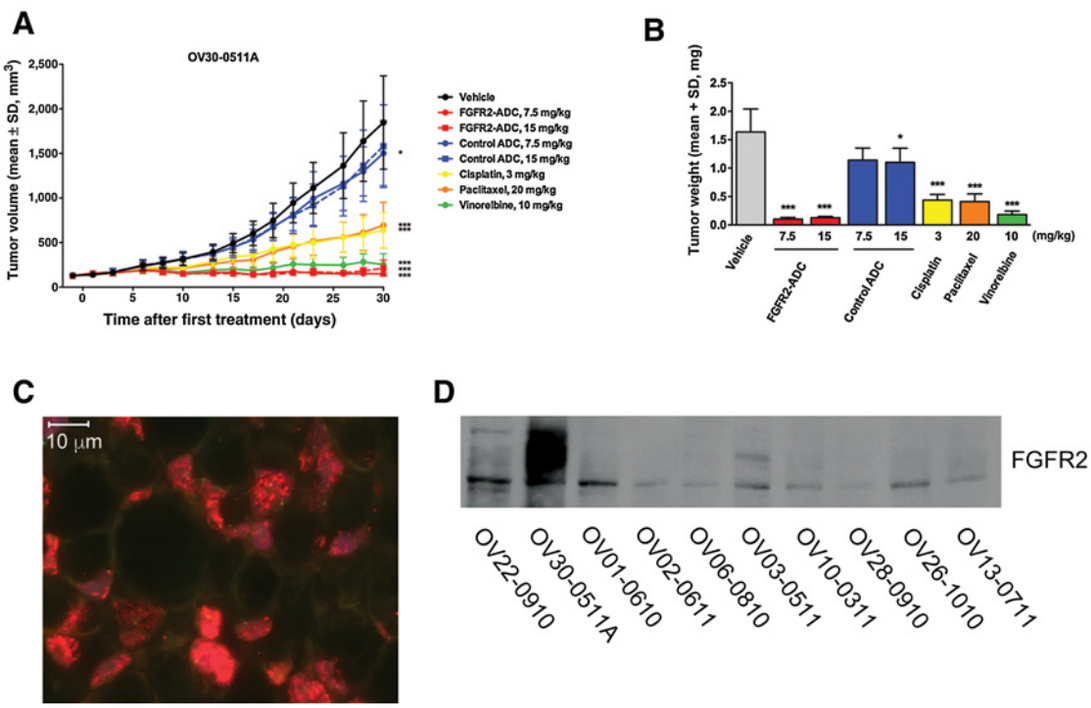

Figure 4.
Antitumor efficacy of FGFR2-ADC BAY 1187982 in OV30-0511A ovarian cancer PDX model. Treatments with FGFR2-ADC (BAY 1187982, DAR of 4.0), control ADC, cisplatin, paclitaxel, and vinorelbine were initiated when tumors had reached a size of approximately 150 mm^3. **A,** tumor growth ($n = 30$). Statistical analysis was performed by Kruskal–Wallis test, followed by Mann–Whitney *U* test. *, $P < 0.05$; ***, $P < 0.001$. **B,** final tumor weight 30 days after first treatment. Comparisons were performed by Kruskal–Wallis test. *, $P < 0.05$; ***, $P < 0.001$. **C,** FISH experiments with probes for *FGFR2* (red), which is located on chromosome 10, and the centromeric region of chromosome 10 (*CEN10*, green) demonstrates *FGFR2* amplification in OV30-0511A model. **D,** immunoblot indicates a high level of FGFR2 protein expression in the OV30-0511A model.

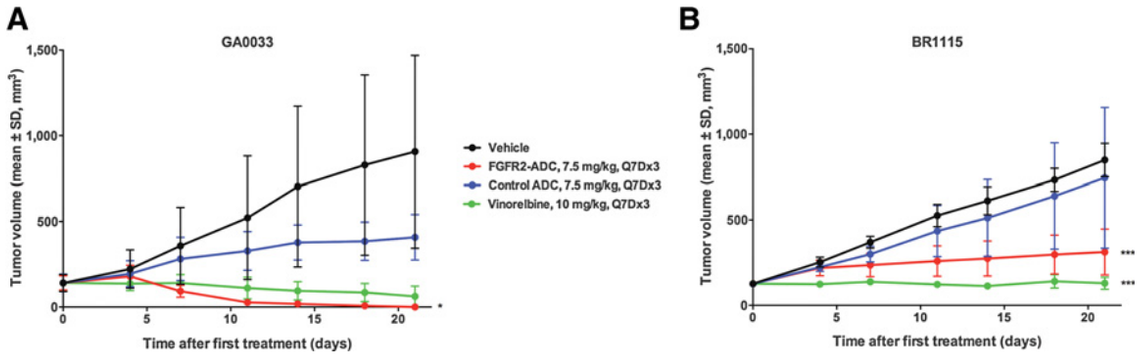

Figure 5.

Antitumor efficacy of FGFR2-ADC BAY 1187982 in gastric and breast cancer PDX models. **A** and **B,** treatments with FGFR2-ADC (BAY 1187982, DAR of 4.1), control ADC, and vinorelbine were initiated when tumors had reached a size of approximately 150 mm^3. **A,** tumor growth in the gastric cancer model GA0033 ($n = 5$). **B,** tumor growth in the breast cancer PDX model BR1115 ($n = 5$). Comparisons were performed at end point using one-way ANOVA, followed by Tukey HSD. *, $P < 0.05$; ***, $P < 0.001$. Q7D×3, every 7th day for three cycles.

The potent antitumor efficacy of BAY 1187982 at 7.5 mg/kg was apparent in GA0033 gastric cancer PDX model with high FGFR2 expression ($P = 0.0267$, Fig. 5A). Tumor eradication was achieved in all mice (5 of 5) treated with BAY 1187982, whereas no tumor growth inhibition was observed in mice treated with the control ADC ($P = 0.1667$).

Furthermore, BAY 1187982 at 7.5 mg/kg resulted in strong inhibition of tumor growth in an FGFR2-positive BR1115 breast cancer model with a T/C ratio of 0.37 ($P < 0.001$, Fig. 5B). In contrast, no effect on tumor growth was observed for the control ADC indicating high selectivity of BAY 1187982.

Importantly, the unconjugated FGFR2-Ab was not efficacious in any of the PDX models with T/C ratios 0.97, 1.38, and 1.03 in OV30-0511A, GA0033, and BR1115 models, respectively.

To analyze the mode of action of BAY 1187982 *in vivo*, FFPE samples of the BR1115 model were stained for phospho-histone H3 (pHH3, Ser10) as marker of cells in G_2–M phase, cleaved PARP1 as marker of apoptosis and for α-tubulin to indicate tubulin structures. In BAY 1187982–treated BR1115 tumors, a 2-fold increase of cells with colocalization of α-tubulin–stained mitotic spindles with pHH3 as marker for G_2–M phase chromosomes compared with the control ADC and the vehicle-treated groups was observed, indicating induction of G_2–M phase arrest after specific uptake of BAY 1187982 into FGFR2-positive cells *in vivo*. In both BAY 1187982 and vinorelbine-treated BR1115 tumors, a 4-fold increase of cleaved PARP1-positive tumor cells was detected compared to vehicle or control ADC–treated tumors, indicating that BAY 1187982 induces apoptosis *in vivo* in a comparable range to vinorelbine which has a similar mode of action, that is, microtubule depolymerization.

Taken together, a positive correlation was observed between *FGFR2* amplification and/or mRNA expression and antitumor activity *in vivo* regardless of the cancer type (Table 1). In general, no response *in vivo* is observed with tumor models with no or low FGFR2 expression. Variable responses were observed when models with intermediate *FGFR2* amplification and/or mRNA expression were evaluated.

Discussion

FGFR2 aberrations, such as gene amplifications as well as protein and RNA overexpression, have been implicated in the development and progression of multiple cancer types and are commonly associated with poor prognosis and resistance to cancer treatments (7, 9–11, 13). FGFR2 is highly expressed in several cancers and exhibits only restricted expression in normal tissues and organs, making it a valuable cancer target and an ideal candidate for the development of an ADC. Here, we have generated an FGFR2-specific human monoclonal Ab (BAY 1179470), which binds to FGFR2-IIIb and FGFR2-IIIc. We demonstrate that the unconjugated control Ab can be used to efficiently target FGFR2-expressing tumor cells, resulting in receptor internalization and FGFR2 degradation. However, use of the unconjugated antibody alone is not sufficient to inhibit growth in most FGFR2-positive tumor models tested indicating an FGFR2-independent mode of cell survival in some tumors. Therefore, we utilized the FGFR2-Ab (BAY 1179470) as a targeting moiety and conjugated it via lysine side chains to a novel microtubule-disrupting auristatin W derivative via a noncleavable linker. Here, we provide the first preclinical evidence of the successful use of a highly potent FGFR2-ADC (BAY 1187982) for the treatment of FGFR2-positive tumors.

BAY 1187982 demonstrates antitumor activity in SNU-16 gastric cancer and, importantly, also in MFM-223 TNBC model previously shown to be unresponsive to the unconjugated FGFR2-Ab. This suggests that the specificity and efficacy of BAY 1187982 in eliminating FGFR2-expressing tumor cells is largely due to the action of the conjugated payload.

N,N-Dialkyl auristatin W derivatives are highly efficient microtubule-disrupting agents (23). ADCs employing such payloads were optimized for high potency, selectivity, as well as maximum linker stability to avoid ADC deconjugation *in vivo*. We show that targeted release and intracellular accumulation of BAY 1168650, the non–cell-permeable active metabolite of BAY 1187982, exerts potent cytotoxic effects in several FGFR2-positive tumor models. The mode of action of the toxophore metabolite is shown to be microtubule depolymerization resulting in induction of apoptosis *in vivo* comparable to vinorelbine. Intriguingly, BAY 1187982 also demonstrates activity in tumor models (e.g., the NCI-H716 colorectal cancer model) that are not sensitive to other microtubule-targeting agents such as paclitaxel and vinorelbine.

BAY 1187982 resulted in dose-dependent tumor regression including PRs and CRs in TNBC and gastric cancer, and tumor stasis in *in vivo* models of ovarian cancer and was well tolerated.

Importantly, we observed a positive correlation between FGFR2 protein levels and BAY 1187982 cytotoxic potency *in vitro* (Supplementary Table S1). Similarly, a positive correlation was observed between *FGFR2* amplification and mRNA expression and antitumor activity *in vivo* (Table 1). Consequently, FGFR2 mRNA levels and *FGFR2* gene amplification present themselves as attractive selection markers for patient stratification during clinical development.

Taken together, we report the identification and characterization of BAY 1187982, a potent and selective FGFR2-ADC for treatment of FGFR2-positive human malignancies. Phase I study (NCT02368951) with BAY 1187982 is currently ongoing.

Disclosure of Potential Conflicts of Interest

H. Apeler, M. Braun, F. Dittmer, S. Hammer, R. Jautelat, H.-G. Lerchen, C.F. Nising, F. Reetz, J. Schuhmacher, A. Sommer, and K. Ziegelbauer have ownership interest as shares in Bayer AG. No potential conflicts of interest were disclosed by the other authors.

Authors' Contributions

Conception and design: A. Sommer, C. Kopitz, C.F. Nising, H.-G. Lerchen, B. Stelte-Ludwig, S. Wittemer-Rump, A. Harrenga, F. Dittmer, F. Reetz, H. Apeler, K. Ziegelbauer, B. Kreft

Development of methodology: C. Kopitz, C. Mahlert, H.-G. Lerchen, B. Stelte-Ludwig, S. Hammer, S. Greven, M. Braun

Acquisition of data (provided animals, acquired and managed patients, provided facilities, etc.): A. Sommer, C. Kopitz, C.A. Schatz, C.F. Nising, C. Mahlert, B. Stelte-Ludwig, S. Hammer, S. Greven, J. Schuhmacher, A. Harrenga, H. Huynh

Analysis and interpretation of data (e.g., statistical analysis, biostatistics, computational analysis): A. Sommer, C. Kopitz, C.A. Schatz, C.F. Nising, C. Mahlert, B. Stelte-Ludwig, S. Hammer, S. Greven, J. Schuhmacher, M. Braun, H. Zierz, A. Harrenga, H. Apeler

Writing, review, and/or revision of the manuscript: A. Sommer, C. Kopitz, C.F. Nising, C. Mahlert, B. Stelte-Ludwig, S. Hammer, J. Schuhmacher, M. Braun, S. Wittemer-Rump, A. Harrenga, F. Dittmer, F. Reetz, H. Apeler, K. Ziegelbauer, B. Kreft

Administrative, technical, or material support (i.e., reporting or organizing data, constructing databases): B. Stelte-Ludwig, S. Hammer

Study supervision: A. Sommer, C. Kopitz, B. Stelte-Ludwig, R. Jautelat, K. Ziegelbauer, B. Kreft

Other [*as a chemist in the project, he designed and synthesized the ADC molecule (payload-linker synthesis and conjugation)*]: H.-G. Lerchen

Acknowledgments

We thank Anna Behnke, Susanne Bendix, Sandra Berndt, Tim Brandenburger, Henryk Bubik, Anna DiBetta, Norman Dittmer, Karola Henschel, Sabine Jabusch, Katrin Jänsch, Beate König, Nadja Langner, Stefanie Mai, Bettina Muchow, Jenny Stepan, Rukiye Tamm, Jan Tebbe, Bianka Timpner, Simone Zolchow, Nina Wobst, and Dirk Wolter for excellent technical assistance. We thank Seattle Genetics Inc. for their support and Aurexel Ltd. (www.aurexel.com) for editorial support funded by Bayer Pharma AG.

Grant Support

This work was supported by a grant from the National Medical Research Council of Singapore (NMRC/MOHIAFCat1/0002/2014) to Hung Huynh.

The costs of publication of this article were defrayed in part by the payment of page charges. This article must therefore be hereby marked *advertisement* in accordance with 18 U.S.C. Section 1734 solely to indicate this fact.

Received January 18, 2016; revised June 29, 2016; accepted August 1, 2016; published OnlineFirst August 19, 2016.

References

1. Sievers EL, Senter PD. Antibody-drug conjugates in cancer therapy. Annu Rev Med 2013;64:15–29.
2. Mack F, Ritchie M, Sapra P. The next generation of antibody drug conjugates. Semin Oncol 2014;41:637–52.
3. Mullard A. Maturing antibody-drug conjugate pipeline hits 30. Nat Rev Drug Discov 2013;12:329–32.
4. Chari RV, Miller ML, Widdison WC. Antibody-drug conjugates: an emerging concept in cancer therapy. Angew Chem 2014;53:3796–827.
5. Miller ML, Fishkin NE, Li W, Whiteman KR, Kovtun Y, Reid EE, et al. A new class of antibody-drug conjugates with potent DNA alkylating activity. Mol Cancer Ther 2016;15:1870–8.
6. Wesche J, Haglund K, Haugsten EM. Fibroblast growth factors and their receptors in cancer. Biochem J 2011;437:199–213.
7. Andre F, Cortes J. Rationale for targeting fibroblast growth factor receptor signaling in breast cancer. Breast Cancer Res Treat 2015;150:1–8.
8. Carter EP, Fearon AE, Grose RP. Careless talk costs lives: fibroblast growth factor receptor signalling and the consequences of pathway malfunction. Trends Cell Biol 2015;25:221–33.
9. Deng N, Goh LK, Wang H, Das K, Tao J, Tan IB, et al. A comprehensive survey of genomic alterations in gastric cancer reveals systematic patterns of molecular exclusivity and co-occurrence among distinct therapeutic targets. Gut 2012;61:673–84.
10. Dienstmann R, Rodon J, Prat A, Perez-Garcia J, Adamo B, Felip E, et al. Genomic aberrations in the FGFR pathway: opportunities for targeted therapies in solid tumors. Ann Oncol 2014;25:552–63.
11. Kim S, Dubrovska A, Salamone RJ, Walker JR, Grandinetti KB, Bonamy GM, et al. FGFR2 promotes breast tumorigenicity through maintenance of breast tumor-initiating cells. PLoS One 2013;8:e51671.
12. Martignetti JA, Camacho-Vanegas O, Priedigkeit N, Camacho C, Pereira E, Lin L, et al. Personalized ovarian cancer disease surveillance and detection of candidate therapeutic drug target in circulating tumor DNA. Neoplasia 2014;16:97–103.
13. Turner N, Grose R. Fibroblast growth factor signalling: from development to cancer. Nat Rev Cancer 2010;10:116–29.
14. Turner N, Lambros MB, Horlings HM, Pearson A, Sharpe R, Natrajan R, et al. Integrative molecular profiling of triple negative breast cancers identifies amplicon drivers and potential therapeutic targets. Oncogene 2010;29:2013–23.
15. Maderna A, Leverett CA. Recent advances in the development of new auristatins: structural modifications and application in antibody drug conjugates. Mol Pharm 2015;12:1798–812.
16. Lerchen H-G, Hammer S, Harrenga A, Kopitz CC, Nising CF, Sommer A et al., inventors. FGFR antibody drug conjugates (ADCs) and the use thereof. Patent WO2013087716 A3. 2013 Aug 22.
17. Carlsson R, Soderlind E. n-CoDeR concept: unique types of antibodies for diagnostic use and therapy. Expert Rev Mol Diagn 2001;1:102–8.
18. Söderlind E, Strandberg L, Jirholt P, Kobayashi N, Alexeiva V, Aberg AM, et al. Recombining germline-derived CDR sequences for creating diverse single-framework antibody libraries. Nat Biotechnol 2000;18:852–6.
19. Wang F, Flanagan J, Su N, Wang LC, Bui S, Nielson A, et al. RNAscope: a novel *in situ* RNA analysis platform for formalin-fixed, paraffin-embedded tissues. J Mol Diagn 2012;14:22–9.
20. Eisenhauer EA, Therasse P, Bogaerts J, Schwartz LH, Sargent D, Ford R, et al. New response evaluation criteria in solid tumours: revised RECIST guideline (version 1.1). Eur J Cancer 2009;45:228–47.
21. Lee J, Kim S, Kim P, Liu X, Lee T, Kim KM, et al. A novel proteomics-based clinical diagnostics technology identifies heterogeneity in activated signaling pathways in gastric cancers. PLoS One 2013;8:e54644.
22. Shen BQ, Xu K, Liu L, Raab H, Bhakta S, Kenrick M, et al. Conjugation site modulates the *in vivo* stability and therapeutic activity of antibody-drug conjugates. Nat Biotechnol 2012;30:184–9.
23. Lerchen H-G, Stelte-Ludwig B, Golfier S, Schuhmacher J, Krenz U, inventors. Novel auristatin derivatives and use thereof. Patent WO2011154359. 2011 Dec 15.